

## Modified Multiport Dc-Dc Converter Topology For Smart Grid

Dhamodharan Shanmugam, Dhivya Balakrishan, K.Indiradevi

<sup>1</sup>M.E-PED, Department OF EEE, Sri Shakthi Institute of Engineering and Technology, Coimbatore, Tamilnadu. INDIA.

<sup>2</sup>M.E-PED, Department OF EEE, Sri Shakthi Institute of Engineering and Technology, Coimbatore, Tamilnadu. INDIA.

<sup>3</sup>Asst.Prof (S)/Department OF EEE, Sri Shakthi Institute of Engineering and Technology, Coimbatore, Tamilnadu. INDIA.

**Abstract:** - The development of a Solid State Transformer (SST) that incorporates a DC-DC multiport converter to integrate both photovoltaic (PV) power generation and battery energy storage is presented in this dissertation. The DC-DC stage is based on a quad active-bridge (QAB) converter which not only provides isolation for the load, but also for the PV and storage. The AC-DC stage is implemented with a pulse-width-modulated (PWM) single phase rectifier. A unified gyrator-based average model is developed for a general multi-active-bridge (MAB) converter controlled through phase-shift modulation (PSM). Expressions to determine the power rating of the MAB ports are also derived. The developed gyrator-based average model is applied to the QAB converter for faster simulations of the proposed SST during the control design process as well for deriving the state-space representation of the plant. Both linear quadratic regulator (LQR) and single-input-single-output (SISO) types of controllers are designed for the DC-DC stage. A novel technique that complements the SISO controller by taking into account the cross coupling characteristics of the QAB converter is also presented herein. Cascaded SISO controllers are designed for the AC-DC stage. The QAB demanded power is calculated at the QAB controls and then fed into the rectifier controls in order to minimize the effect of the interaction between the two SST stages. The dynamic performance of the designed control loops based on the proposed control strategies are verified through extensive simulation of the SST average and switching models.

**Keywords:-** DC-DC converter, distributed generation, multiport converter, smart grid, solid-state transformer.

### I. INTRODUCTION

In the last decade, the Smart Grid concept has drawn the attention of researchers and industry as a feasible solution to the challenges that the entire electrical system is facing due to the growth in load, the increasing penetration of renewables and the deployment of the distributed generation at the consumer end [1]. Currently, the Future Renewable Electric Energy Delivery and Management (FREEDM) Systems Center is working in several areas in its efforts to contribute with the modernization of the power distribution system and help develop the standards for the implementation and optimal operation of this portion of the future Smart Grid [2]. The power-electronics-based transformer, or so-called SST, is one of the key components of the FREEDM distribution system. In addition to serving as a regular distribution transformer, the SST provides ports for the proper integration of distributed energy resources (DER) and distributed energy storage (DES), thus enhancing the reliability of the distribution system [3]. Additionally, the SST enables the implementation of distributed intelligence through a secure communication network (COMM) to ensure stability and optimal operation of the distribution system. Another important component of the FREEDM distribution system is the Fault Identification Device (FID), which is a fast protection device deployed to enable Intelligent Fault Management (IFM) [4].

Besides the advantage of its reduced size and weight due to its high frequency (HF) transformer [5], the SST makes use of state-of-the-art Power Electronics devices that allows it to provide additional functionalities such as on-demand reactive power support to grid, power quality, current limiting, storage management and a DC bus for end use. Poor load power factor and harmonics are isolated from the distribution system, thus improving the overall system efficiency. Additionally, the selection of new generation materials for semiconductors and magnetics may help improve its efficiency when compared to a regular transformer of the

same ratings. Fig. 1 shows the SST interfacing photovoltaic (PV) generation, storage, electric loads as well as plug-in hybrid electric vehicles (PHEV).

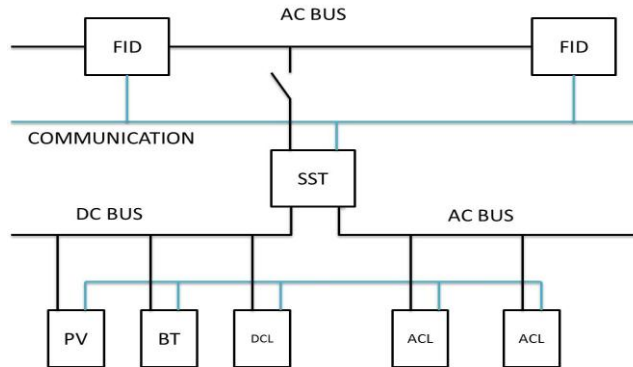


Figure. 1. Integration of DES, DER and intelligent loads through the SST.

The interest in renewable sources of energy has increase, considerably. They represent a potential solution to mitigate environmental issues and reduce the dependence on traditional sources of energy for electrical generation. The need of technology for adapting these non-traditional types of energy into the system has motivated the development of new generation power electronics converters. The future homes will make use of power converters to integrate all the available sources of electrical energy, including renewables as wind turbine (WT) and PV. These power converters have to meet efficiency, flexibility, power density, reliability and safety requirements.

A generation of power converters that has been proposed by researchers for the integration of distributed generation (DG) and storage is the family of multi-port DC-DC converters [6]. Their advantage lies in the integration of several sources with minimum DC-DC conversion stages. The traditional and integrated configurations introduced in [6] are shown in Fig. 2 and Fig. 3, respectively. The latter may require a reduced the number of components while providing galvanic isolation.

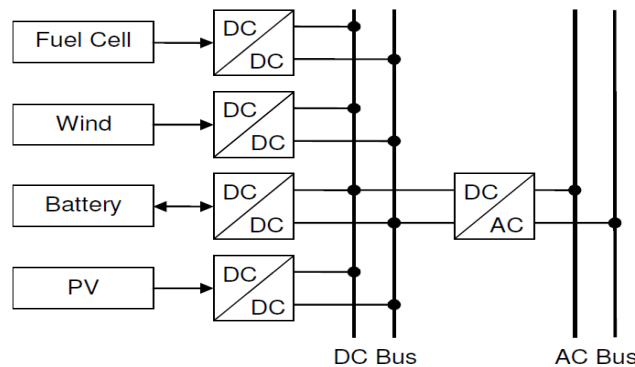


Figure. 2. Conventional power conversion through two-port DC-DC converters.

Since the SST and the multi-port converters are two key areas of research, the work presented herein has been motivated by the better integration that the SST can achieve with the use of multi-port converters. The three-stage configuration that has been identified as a potential candidate for the SST implementation relies on a DC bus for PV and storage integration.

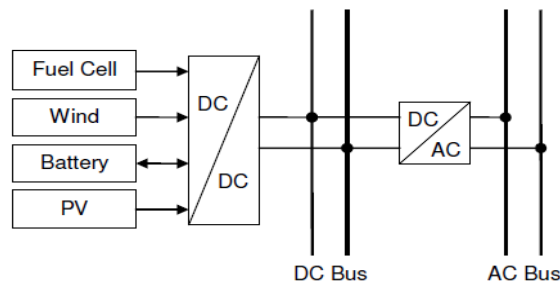


Figure. 3. Integrated power conversion through a multi-port DC-DC converter

This is achieved through separate DC-DC converters. Without isolation, the voltage ratings of these devices must be selected mainly based on the DC bus voltage rating. If voltage ratings are not compatible and/or isolation is required, then additional isolation is needed, thus increasing the size of the system. Furthermore, separate controllers for each DC-DC converter are to be designed. In this design process, the stability of the interconnected DC-DC converters must be ensured. The need of technology for integrating DG and storage into the distribution system has motivated the development of a new generation of power converters. A family of multiport dc–dc converters, which includes the multiactive-bridge (MAB) converters, has been proposed by researchers [6]. Their advantage lies in the integration of several sources with minimum dc–dc conversion stages, which yields a higher power density. Since the SST considered herein includes the grid, the load, the PV system, and the storage, a four-port dc–dc converter as the quad-active-bridge (QAB) converter is required.

**II. PROPOSED SYSTEM**

This paper proposes the development of a SST based on a QAB converter, to integrate DG and storage. The QAB converter, used in the implementation of the SST dc–dc stage, provides isolation for DG and storage through a single four-winding HF transformer as seen in Fig. 4 and the control design involves the analysis of only a single converter. The proposed SST is based on a particular type of multi-port converter, called quad-active-bridge (QAB) converter, to integrate PV and storage. This SST topology eliminates the need of additional isolation and only an integrated controller for the DCDC stage may be required.

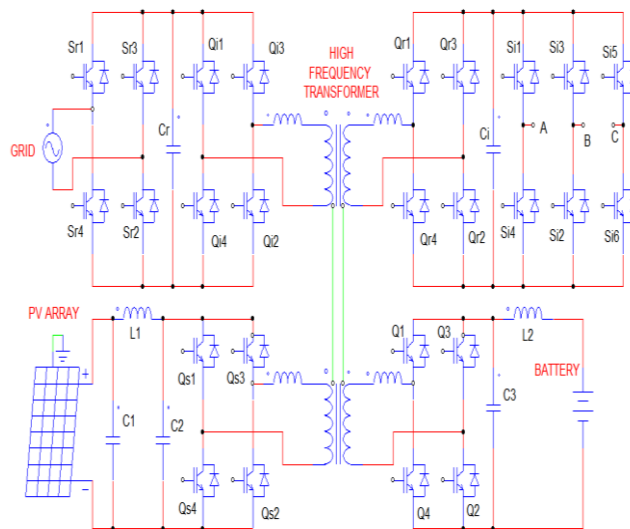


Figure 4. QAB-based SST with PV and storage integrated through HF transformer.

The block representation of the proposed SST topology is shown in Fig. 5. Since little information is available on the literature for the QAB converter, a detailed analysis is required. Furthermore, an average model for any multi-active-bridge (MAB) converter is developed and expressions to calculate the rated power of any MAB port are derived. This is the basis for the dynamic analysis and control design of the DC-DC stage of the proposed SST topology.

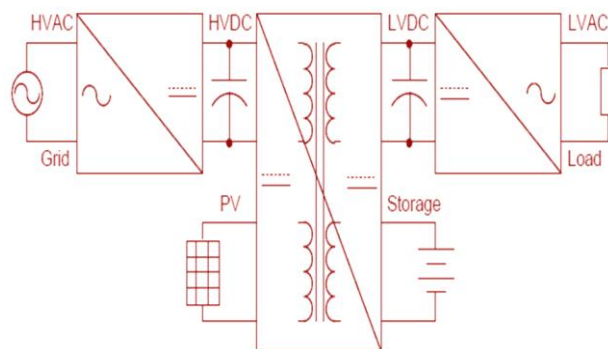


Figure 5. QAB-based SST with storage and PV.

The control design for the SST DC-DC stage is performed using both the conventional single-input-single-output (SISO) approach and a more modern multiple input- multiple-output (MIMO) approach. Furthermore, the SISO controller is complemented with a novel technique to deal with the cross-coupled characteristics of the QAB. Additionally, the control design for the SST AC-DC stage introduces a technique to deal with the interactions that result when the above two SST stages are interconnected. The performance of the controls is verified through extensive simulation of both switching and average models of the SST. Experimental results from the hardware implementation of a prototype SST are presented for validation purposes. Since no contributions are made on the SST DC-AC stage, it is modeled with a current source during its analysis and simulation, and implemented with an electronics load when testing the prototype SST.

**III. QAB CONVERTER**

Since the QAB converter has been selected for the implementation of the SST dc-dc stage, it will be analyzed herein following the approach developed for the MAB converter in the previous section. In [7], the authors briefly introduce the QAB converter; however, no experimental results have been provided to date. The switching model of the QAB converter is shown in Fig. 4 while its “Δ” equivalent ac circuit referred to port 1 is shown in Fig. 6, where the involved link inductances can be calculated with (1). Based on Fig. 6, the idealized steady-state QAB waveforms for unity-dc-conversion ratios are illustrated in Fig. 7. The bottom two plots show the currents *ij* at the dc side of the QAB ports, along with their corresponding CCA values *Ij*. The involved gyration gains can be calculated by using (2). When the max QAB link power has been reached between any two ports, the direction of the QAB power flow depends on the number of source, forwarding, and load ports [8] – [15].

$$L_{jk} = (L'_j + L_{THj}) \left[ L'_k \left( \frac{1}{L_m} + \sum_{l \neq j,k} \frac{1}{L'_l} \right) + 1 \right] \dots\dots\dots(1)$$

$$g_{jk} = \frac{I_{jk}}{V_k} = \frac{N_1^2}{N_j N_k} \frac{1}{2\pi f_s L_{jk}} \phi_{jk} \left( 1 - \frac{|\phi_{jk}|}{\pi} \right) \dots\dots\dots(2)$$

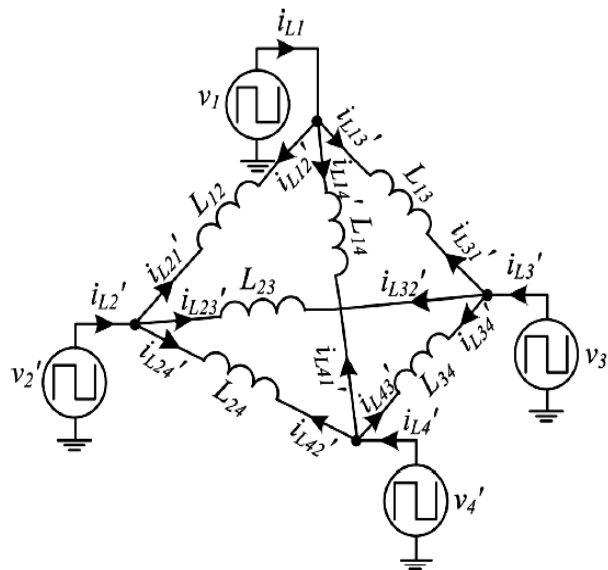


Figure 6. QAB “Δ” equivalent ac circuit referred to port 1.

**IV. CONTROL SYSTEM**

The block diagram in Fig. 8 shows the single-input-single output type of control loop for the PV voltage implemented herein. The gains associated with the feedback-signal conditioning, as well as the DSP digital-to-analog conversion and pulse width modulation (PWM) modules have been intentionally omitted for simplicity.

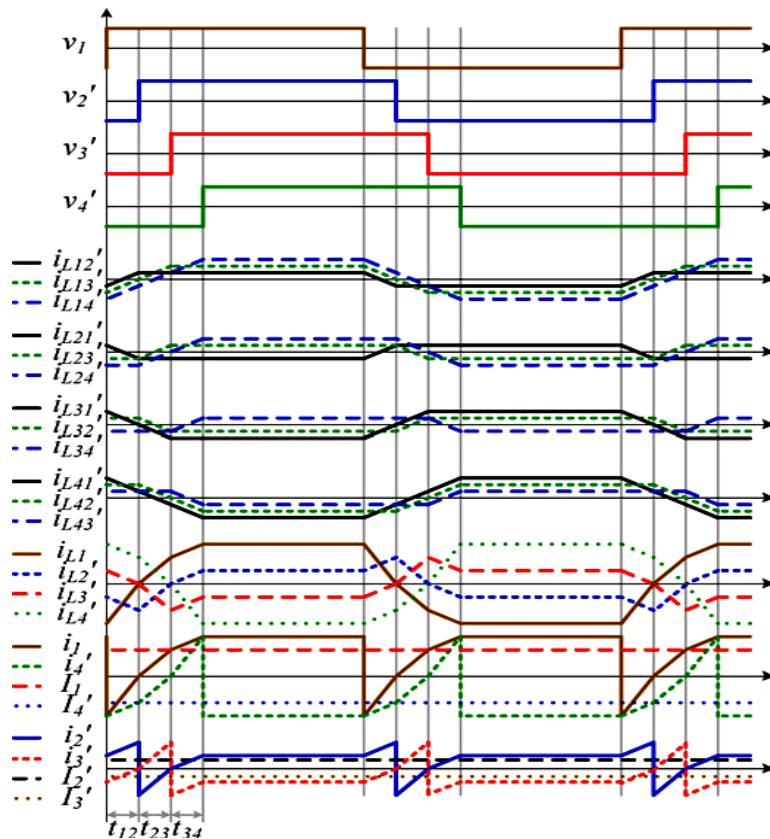


Figure 7. Idealized steady-state QAB switching waveforms for unity-dc conversion ratios and equal link inductances.

The control loops for the LVDC voltage and the battery current share the same structure. In the event that its saturation limits implemented on the DSP are reached, a controller may try to drive the phase-shift angles of the slower loops through the entries of the *KB* matrix. In order to avoid this, it may require forcing *KB* to be the identity matrix.

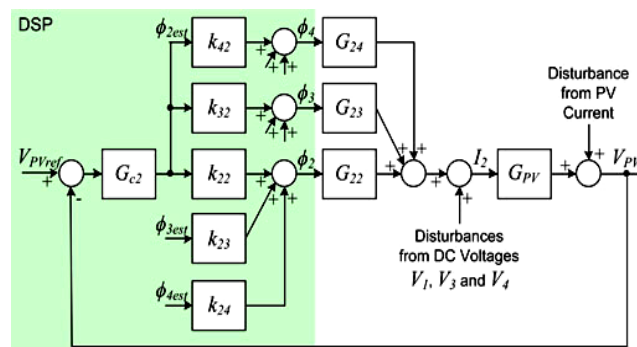


Figure 8. Simplified PV voltage control loop.

The entries of *GC* have been designed with the k-factor technique [16] with bandwidths of 200, 20, and 2 Hz for *Gc3*, *Gc2*, and *Gc4*, respectively, and phase margin of 60° for all of them. Alternatively, a multiple-input multiple- output type of control loop can be considered in order to incorporate the dc voltages as plant state variables [17], [18].

### V. SIMULATION RESULTS

The selected simulation package is MATLAB/Simulink complemented with PLECS block set. Based on Fig. 4, the system electrical parameters are listed in Table I. The base inductance, obtained from the switching frequency, voltage, and current rating, is 76.4 μH. The QAB switching waveforms for  $\varphi_2 = -38^\circ$ ,  $\varphi_3 = -76^\circ$ , and  $\varphi_4 = -38^\circ$  are shown in Fig. 9.

TABLE I: SYSTEM ELECTRICAL PARAMETERS

Description	Symbol	Value
High-voltage-DC link voltage	$V_{HVDC}$	48 V
Low-voltage-DC link voltage	$V_{LVDC}$	48 V
PV voltage	$V_{PV}$	48 V
Battery voltage	$V_{Batt}$	48 V
Ports Current Rating	$I_{Rating}$	5 A
Port 1 leakage inductance	$L_1$	0.851 pu
Port 2 leakage inductance	$L_2$	0.851 pu
Port 3 leakage inductance	$L_3$	0.851 pu
Port 4 leakage inductance	$L_4$	0.851 pu
CLC filter inductance	$L_{F1}$	0.151 pu
LC filter inductance	$L_{F2}$	0.191 pu
High-voltage-DC link capacitance	$C_{HVDC}$	200 $\mu$ F
CLC filter capacitance 1	$C_{F1}$	200 $\mu$ F
CLC filter capacitance 2	$C_{F2}$	200 $\mu$ F
Low-voltage-DC link capacitance	$C_{F3}$	200 $\mu$ F
LC filter capacitance	$C_{F4}$	200 $\mu$ F
Maximum phase-shift angle	$\phi$	90°
Switching frequency	$f_s$	20 kHz

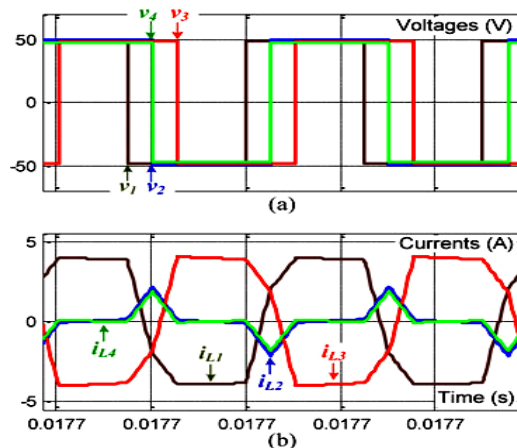


Fig. 9. Simulation results: QAB steady-state switching waveforms for  $\phi_2 = -38^\circ$ ,  $\phi_3 = -76^\circ$ , and  $\phi_4 = -38^\circ$ .

For the simulation of the close-loop operation, a step load at the LVDC link is applied to the system. The transient response when  $KB$  equals the identity matrix is seen in Fig. 10. It can be observed that, following the disturbance, the power variation is distributed among the remaining ports. This causes the PV voltage to dip. In steady state, the power is balanced by the HVDC link. When  $KB$  is selected to transfer the power variation onto the HVDC port, the transient response is seen in Fig. 11. It can be observed that the current from the HVDC link is forced to increase to meet the current demanded by the load with minimal undershoot on the PV and battery currents.

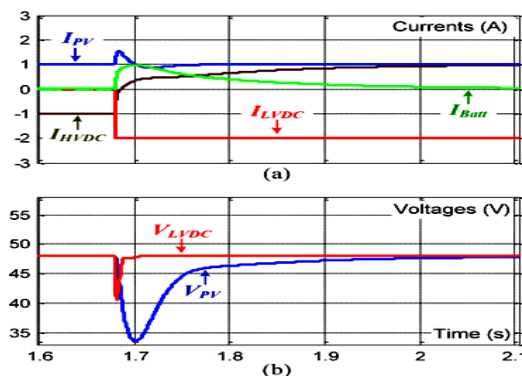


Fig. 10. Simulation results: SST dc–dc stage transient response to a step load when  $KB$  equals the identity matrix.

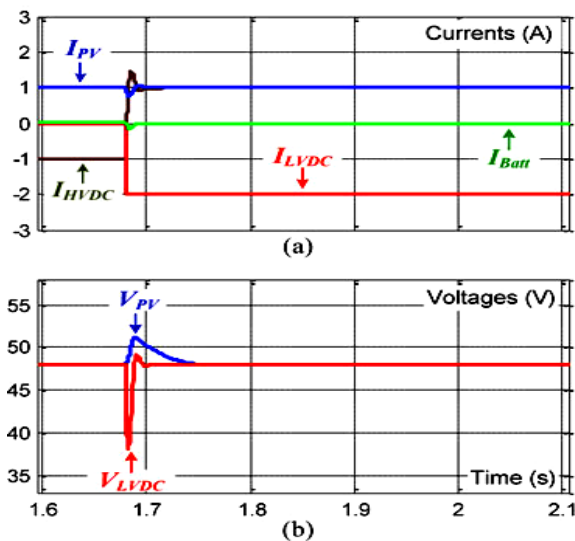


Fig. 11. Simulation results: SST dc–dc stage transient response to a step load when the power variation is transferred onto the HVDC link.

As a result, following the disturbance, the battery is forced to supply the current demanded by the load before slowly returning to its initial steady state. As seen from the simulation results, The QAB dc-side currents are directly controlled through the phase-shift angles both during transients as well as during steady state, thus ensuring the transformer amp-turn balancing at the QAB ac side. During transients, the QAB currents are shared depending on the selection of  $KB$ , as seen in Fig. 10 through Fig. 11. During steady state, the QAB currents are shared depending on the controls set point.

## VI. CONCLUSION

A SST topology based on a QAB converter that provides isolation for the load, as well as DG and storage has been proposed herein. A gyrator-type large-signal average model has been developed for a general MAB converter and used to speed up the simulation of the dc–dc stage of the QAB-based SST. The expressions to determine the power rating of an MAB port have been derived and used to determine the power rating of the QAB ports considering the operating characteristics of the SST application. A control technique that takes into account the cross-coupling characteristics of the QAB converter has been introduced herein. This technique allows improving the dynamic performance of the HVDC voltage regulation of the SST. The dynamic performance of the control strategy has been verified through extensive simulation of both switching and average models.

## REFERENCES

- [1] Hassan, R.; Radman, G.; , "Survey on Smart Grid," *IEEE SoutheastCon 2010 (SoutheastCon), Proceedings of the* , vol., no., pp.210–213, 18–21 March 2010.
- [2] Huang, A.Q.; Baliga, J.; , "FREEDM System: Role of power electronics and power semiconductors in developing an energy internet," *Power Semiconductor Devices & IC's, 2009. ISPSD 2009. 21st International Symposium on*, vol., no.pp.9–12, 14–18 June 2009.
- [3] Heydt, G.T.; , "Future renewable electrical energy delivery and management systems: Energy reliability assessment of FREEDM systems," *Power and Energy Society General Meeting, 2010 IEEE* , vol., no., pp.1–4, 25–29 July 2010.
- [4] Karady, G.G.; Xing Liu; , "Fault management and protection of FREEDM systems," *Power and Energy Society General Meeting, 2010 IEEE* , vol., no., pp.1–4, 25–29 July 2010.
- [5] Tiefu Zhao; Liyu Yang; Jun Wang; Huang, A.Q., "270 kVA Solid State Transformer Based on 10 kV SiC Power Devices," *Electric Ship Technologies Symposium, 2007. ESTS '07. IEEE*, vol., no., pp.145–149, 21–23 May 2007.
- [6] Tao, H.; Kotsopoulos, A.; Duarte, J.L.; Hendrix, M.A.M.; , "Family of multiport bidirectional DC-DC converters," *Electric Power Applications, IEE Proceedings -* , vol.153, no.3, pp. 451– 458, 1 May 2006.

- [7] M. Qiang, W. Wei-yang, and X. Zhen-lin, "A multi-directional power converter for a hybrid renewable energy distributed generation system with battery storage," in *Proc. CES/IEEE 5th Int. Power Electron. Motion Control Conf.*, Aug. 14–16, 2006, vol. 3, pp. 1–5.
- [8] G. Wang, S. Baek, J. Elliott, A. Kadavelugu, F. Wang, X. She, S. Dutta, Y. Liu, T. Zhao, W. Yao, R. Gould, S. Bhattacharya, and A. Q. Huang, "Design and hardware implementation of Gen-1 silicon based solid state transformer," in *Proc. 26th Annu. IEEE Appl. Power Electron. Conf. Expo.*, Mar. 6–11, 2011, pp. 1344–1349.
- [9] H. Tao, A. Kotsopoulos, J. L. Duarte, and M. A. M. Hendrix, "Family of multiport bidirectional DC–DC converters," *IEE Proc.—Electric Power Appl.*, vol. 153, no. 3, pp. 451–458, May 2006.
- [10] R. W. A. A. De Doncker, D. M. Divan, and M. H. Kheraluwala, "A three-phase soft-switched high-power-density DC/DC converter for high-power applications," *IEEE Trans. Ind. Appl.*, vol. 27, no. 1, pp. 63–73, Jan./Feb. 1991.
- [11] H. Tao, A. Kotsopoulos, J. L. Duarte, and M. A. M. Hendrix, "A softswitched three-port bidirectional converter for fuel cell and supercapacitor applications," in *Proc. IEEE 36th Power Electron. Spec. Conf.*, Jun. 2005, pp. 2487–2493.
- [12] C. Zhao and J. Kolar, "A novel three-phase three-port UPS employing a single high-frequency isolation transformer," in *Proc. Power Electron. Specialists Conf.*, vol. 6, Jun. 2004, pp. 4135–4141.
- [13] S. Falcones and R. Ayyanar, "Simple control design for a three-port DCDC converter based PV system with energy storage," in *Proc. 25th Annu. IEEE Appl. Power Electron. Conf. Expo.*, Feb. 21–25, 2010, pp. 2149–2153.
- [14] Q. Chen, F. C. Lee, J. Z. Jiang, and M. M. Jovanovic, "A new model for multiple-winding transformer," in *Proc. 25th Annu. IEEE Power Electron. Spec. Conf. Rec.*, Jun. 20–25, 1994, vol. 2, pp. 864–871.
- [15] M. Ehsani, I. Husain, and M. O. Bilgic, "Power converters as natural gyrators," *IEEE Trans. Circuits Syst. I: Fundam. Theory Appl.*, vol. 40, no. 12, pp. 946–949, Dec. 1993.
- [16] N. Mohan, T. M. Undeland, and W. P. Robbins, *Power Electronics: Converters, Applications, and Design*, 2nd ed. New York: Wiley, 1995.
- [17] A. A. Rodriguez, *Analysis and Design of Multivariable Feedback Control Systems*. Tempe, AZ: Control3D, LLC, 2003.
- [18] D. S. Naidu, *Optimal Control Systems*. Boca Raton, FL: CRC Press, 2003.